

LES modelling of flow in a simple airway model

X.Y. Luo^{*}, J.S. Hinton, T.T. Liew, K.K. Tan

Department of Mechanical Engineering, The University of Sheffield, Mappin Street, Sheffield S1 3JD, UK

Received 23 May 2003; received in revised form 28 January 2004; accepted 19 February 2004

Abstract

Detailed information about the flow field pattern is highly important in accurately predicting particle deposition sites in the human airway. Flow in the upper airway during heavy breathing can have a Reynolds number as high as 9300, and therefore presents turbulent features. Although turbulence is believed to have an important effect on the airflow and other transport processes in the bronchial tree, to date both theoretical and numerical studies have predominantly assumed the flow to be laminar. In this paper, transitional/turbulent flow during inspiration is studied using a large eddy simulation (LES) in a single asymmetric bifurcation model of human upper airway. The influence of the non-laminar flow on the patterns and the particle paths is investigated in both 2D and 3D models. Throughout the investigation, comparisons with the laminar and conventional $k-\epsilon$ models for the same configuration and flow conditions are made. The LES model is also carefully validated against published experimental data in a stenotic tube model. The results demonstrate that the LES model is capable of capturing instantaneous eddy formation and flow separation in (almost) laminar, transitional and turbulent flow regimes, and hence may be used as a powerful and practical tool to provide much of the detailed flow information required for tracing the particle trajectories and particle deposition in human airways.

© 2004 IPPEM. Published by Elsevier Ltd. All rights reserved.

Keywords: Airway; Transitional/turbulent flow; LES; CFD; Particle deposition

1. Introduction

Understanding the distribution of deposition of inhaled aerosols in the tracheo-bronchial airways is highly important in promoting therapeutic effects of airborne pharmacological drugs via targeted delivery, such as those used to treat airway inflammation in asthma, as well as to improve risk assessments of ambient contaminants. Excessive retention of inhaled particles has been known to directly cause diseases, such as pneumoconiosis, silicosis and asbestosis. Therefore, it is very useful to be able to model and predict aerosol transport and local deposition characteristics in the human airway.

Although advanced imaging techniques are capable of obtaining the deposition pattern in the airways at a reasonable level of detail, these data still represent

averages over many individual airway branches. An alternative way to investigate the detailed deposition patterns is to use theoretical calculations, which however have often incorporated rather simple approximations for the flow, a recent example is Darquenne and Paiva [6]. In the last decade, computational fluid dynamics (CFD) has been increasingly applied to the study of fluid dynamics and aerosol particle motion in the human respiratory tract [3,4,19,25]. CFD simulations can provide not only 3D flow patterns within the airways, but also detailed particle deposition patterns.

Numerous CFD studies exist which address the problem of air flow and particle deposition in selected airway segments [2,8,12,14–18,33]. Recently, studies by Martonen et al. [25–27] have simulated the fluid dynamics of the airway bifurcation, and have obtained good agreement with experiments by Schreck [34]. However, the influence of turbulence on air flow and particle motion in the upper airway has been neglected in general [10]. It is known that the Reynolds number, Re , in the trachea varies from 800 in light breathing (10

^{*} Corresponding author. Tel.: +44-114-2227752; fax: +44-114-2227890.

E-mail address: x.y.luo@shef.ac.uk (X.Y. Luo).

l/min) to about 9300 in heavy breathing (100 l/min) [20,31]. Therefore, flow in the trachea is highly likely to be turbulent in the high Re regime. Moreover, the presence of the larynx tends to induce disturbances and instabilities into the air stream as it passes through the constricted glottal aperture and vocal folds. Although flow in the first two generations of large tracheo-bronchial airways is likely to be turbulent, inhaled air decelerates in the subsequent generations of airways due to the effect of branching on flow rate. This deceleration results in relaminarisation of the flow in which turbulence dissipates and eventually dies down. The effect of turbulence, and the transition from laminar to turbulent flow as well as relaminarisation, on the air flow and particle motion in the large tracheo-bronchial airways is still unclear.

Turbulent flows are characterised by eddies with a wide range of length and time scales. The largest eddies are typically comparable in size to the characteristic length of the mean flow, while the smallest scales are responsible for the dissipation of turbulent kinetic energy. It is theoretically possible to directly resolve the whole spectrum of turbulent scales using direct numerical simulation (DNS). Indeed, DNS has been successfully used on particle dispersion in temporal mixing layers [21,24] as well as in spatial mixing layer [13]. However, DNS is extremely expensive and requires huge computer power, as the grid density required is proportional to Re^3 . Thus, for high Reynolds numbers and complicated geometries, such as airway bifurcation models, the mesh sizes required for DNS are prohibitive. Traditional turbulent modelling, such as the $k-\epsilon$ approach, is much cheaper but it only solves for the average velocity field, which is insufficient for tracking particle trajectories. However, in a recent study on a human oral airway model, it has been demonstrated that the main features of laminar–transitional–turbulent particle suspension flows can be captured by using renormalization group (RNG) $k-\epsilon$ model [37], which has to be carefully tuned.

In this paper, large eddy simulation (LES) is employed to study the possible influences of transitional and turbulent airway flow on particle deposition. LES employs an alternative approach in which the large eddies are computed in a time-dependent simulation that uses a set of ‘filtered’ equations. The assumptions behind LES are that momentum, mass, energy and other passive scalars are transported by large eddies. These are more problem dependent and are dictated by the geometries and boundary conditions of the flow involved. To the best of our knowledge, this is the first attempt to simulate transitional/turbulent flow in the asymmetric upper airway model using LES. Here, we primarily focus on validating LES as a feasible model in modelling turbulence in the tracheo-bronchial airways, and compute the correspond-

ing particle paths as a crude prediction of the flow and dispersion of particles under the influence of turbulence. Transitional/turbulent flow is investigated numerically in both 2D and 3D asymmetric models using the commercial CFD package, Fluent 5.3. Differences in results between the LES, laminar and $k-\epsilon$ models are addressed. The model is also validated with the experimental data for a constricted tube by Ahmed and Giddens [1].

The layout of this paper is as follows. Detailed CFD modelling is introduced in Section 2; this includes the assumptions, the model geometries, turbulence modelling, the boundary conditions, and detailed CFD validations. Results of the flow patterns and path lines using LES, $k-\epsilon$, and laminar models are presented in Section 3. Discussions and conclusions are given in Sections 4 and 5.

2. CFD modelling

We are seeking to model only part of the whole breathing cycle, namely (almost) steady inspiration, as occurs when an inhaler is used by a patient. Olson et al. [30] showed in experiments that steady flow can ‘accurately mimic’ conditions during inspiration for flow rates up to 150 l/min. Thus, we assume that the basic flow at the entrance of our model of the airway is a steady plug flow. The air is taken to be incompressible because flow speeds are much slower than the speed of sound, and the temperature and density are assumed to be constant.

2.1. The geometric model

The models are based on human airway casts by Schlesinger and Lippmann [33], where the dimensions were obtained from the autopsy specimens of the human trachea and lungs, with no gross abnormalities. The initial casts have several generations of bifurcations, but due to the extensive computing requirements, our model consists of only the trachea and the right and left bronchi. Their dimensions are summarised in Table 1.

The 2D and 3D models generated from the parameters in Table 1 are shown in Figs. 1 and 2, respectively. The dimensions of the 2D model have been adopted so that it is equivalent to the central cross-sectional projection of the 3D model.

2.2. Turbulence modelling

Three numerical methods are employed, laminar flow, $k-\epsilon$ model, and LES. The governing equations for LES are obtained by filtering the time-dependent Navier–Stokes equations in configuration (physical)

Table 1
Dimensions used for the model based on casts by Schlesinger and Lippmann [33]

	Diameter ^a (cm)	Length (cm)	Angle ^b (degree)
Trachea	2.17	9.2	
Right bronchi	1.7	4.2	15
Left bronchi	1.26	5.3	30

^a These values represent the mean of transverse diameters at the midpoint of each branch.

^b These values represent the angle of branching between the indicated branch and its parent branch.

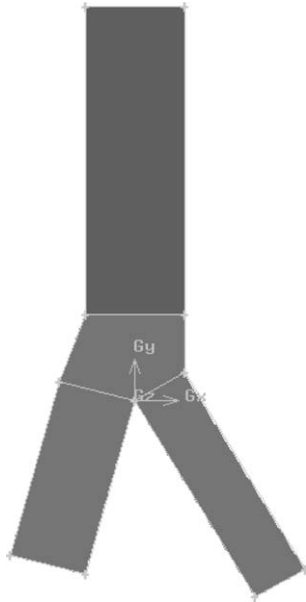


Fig. 1. Two-dimensional model.

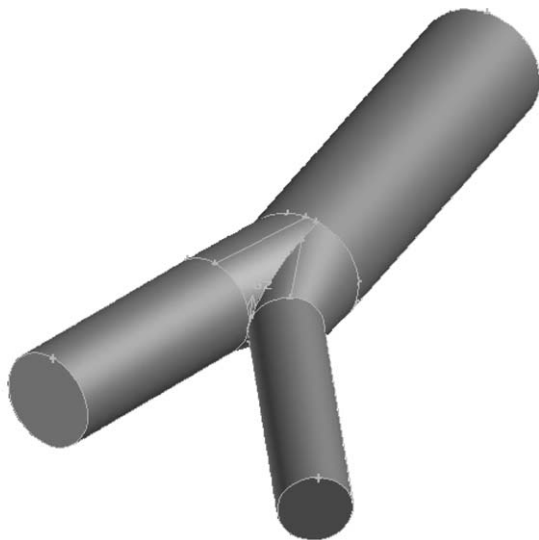


Fig. 2. Three-dimensional model.

space. The process effectively filters out those eddies whose scales are smaller than the grid spacing. The resulting equations thus govern the dynamics of large eddies. Therefore, LES generates an approximation to the real flow in which scales below a certain size are missing. This is corrected by having additional terms in the equation of motion, known as subgrid terms, which only come into play at the smaller of the scales resolved by the LES. Details of the LES modelling are given in Appendix A.

2.3. Boundary conditions

For the laminar model, the boundary conditions are that the velocity, \bar{u} , satisfies the no slip condition at the wall, the velocity at the inlet is uniform, $\bar{u} = \bar{U}_{avg}$, and zero pressure at the outlets.

In the LES model, all the boundary conditions are the same as the laminar model, except that we need to specify the intensity of the small-scale turbulence at the inlet. This is achieved by specifying the amplitude of the velocity fluctuations at the inlet

$$\bar{u} = \bar{U}_{avg}(1 + I\psi) \tag{2.1}$$

where ψ is a Gaussian random number with zero mean and standard deviation equal to one, and I is the intensity of the fluctuation given by

$$I \equiv \frac{\bar{u}'}{\bar{U}_{avg}}, \tag{2.2}$$

where u' is the root-mean-square of the velocity fluctuation. Typical value of I is chosen to be between 5% and 10%. There is no noticeable difference in the results if I is varied in the range.

In the $k-\epsilon$ model, we need to specify the turbulence length scale, l_s , as well as I . I is given by (2.2), and l_s is taken to be the inlet diameter of the model.

2.4. Numerical schemes and parameters

A second order segregated SIMPLE solver [11] is used to solve the governing equations. The solution process is iterative and a convergence criterion is required. In this study, convergence for the laminar and $k-\epsilon$ models is deemed to be achieved when

$$\frac{\|u_{ij}^k - u_{ij}^{k-1}\|}{\bar{U}_{avg}} \leq 10^{-4} \tag{2.3}$$

for all variables i at node points j , and iterations k . As LES is a time-dependent mode, the convergence is determined by monitoring both the residuals and the force coefficients. Convergence is achieved when the

Table 2

The model parameter. Note that Re is the Reynolds number defined as $\rho U_{\text{avg}} D / \mu$, where U_{avg} and D are the maximum velocity and diameter at the entrance to the trachea

Operating pressure	101 kPa
Physical properties	
Density, ρ	1.19 kg/m ³
Viscosity, μ	1.82×10^{-5} kg/ms ⁻¹
No. of nodes/cells in 2D model	21 367/14 493
No. of nodes/cells in 3D model	476 384/88 564
Inspiratory rate	45 l/min
Inlet velocity	2.03 m/s
Re	3012

force coefficients are statistically steady in addition to satisfying (2.3). The time step used in LES modelling is determined by performing numerical tests. In this study, a time step of 0.006 s was found to be sufficient to produce results independent of the choice of time step.

A summary of the physical parameters used is given in Table 2. Triangle/tetrahedral cells are used in the 2D/3D models for their flexibility in adapting to curved surfaces. A mesh boundary layer was also imposed on the wall of the model so that the mesh density can be increased to sufficiently resolve the boundary layer, without substantially increasing the total number of nodes.

The computations were performed using the CFD software Fluent 5 on a SUN Enterprise UNIX network with 5 GB of memory and a maximum speed of 336 MHz. Approximately 3 h are needed for typical runs for the 2D LES models, while more than 30 h are needed for typical runs in the 3D LES models.

2.5. CFD validations

2.5.1. Grid independence test

Grid independence was achieved by using a solution-adaptive refinement, as cells can be added where they

are needed in the mesh. The initial grid was adapted by putting more cells in the areas where the velocity gradient is higher than a chosen level. This process was repeated until the results became grid independent. Fig. 3 shows three 2D meshes: Mesh (a) of 8383 nodes, Mesh (b) of 14 493 nodes, and Mesh (c) of 18 614 nodes. Mesh (b) was chosen since the results in Mesh (b) and Mesh (c) are virtually identical. The same procedure was used for the 3D grids. The number of nodes of the final grids for 2D and 3D models is listed in Table 2.

2.5.2. Comparison with experimental measurements

As there are no experimental data available for flow in the human upper airway model investigated here, the velocity field in an axisymmetric constricted tube (stenosis model) measured by Ahmed and Giddens [1] for $Re = 2000$ was used to validate the LES simulation. The unobstructed diameter of the stenosis model is 0.0508 m, the profile of the stenosis is chosen to be the same as Deshpande et al. [7] and Smith [35], and the grid with 248 841/227 981 nodes/cells is shown in Fig. 4.

The turbulent parameters, boundary and initial conditions are calculated as described in Section 2. The turbulent intensity is taken to be 6.18%, the same as in the experiment [1].

The normalized centreline velocity, V_x/\bar{V} , from the laminar, $k-\epsilon$ and LES simulations is compared with the experimental data in Fig. 5, where \bar{V} is the average inlet velocity for this problem. It seems that in the flow region before the stenosis, all three models agree with each other. They differ as the flow separates downstream of the stenosis. The laminar flow model obviously cannot account for the extensive turbulent energy dissipation downstream, while the $k-\epsilon$ model assumes too much energy dissipation and fails to give the secondary peak in the profile. Although the accuracy of LES is limited by the smallest grid size that can be used (as indicated by a small discrepancy with the

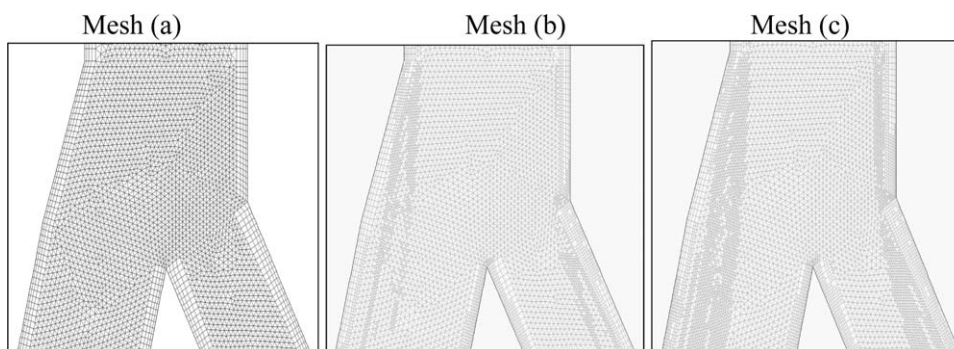


Fig. 3. Grid independence tests were carried out on three different meshes (a)–(c).

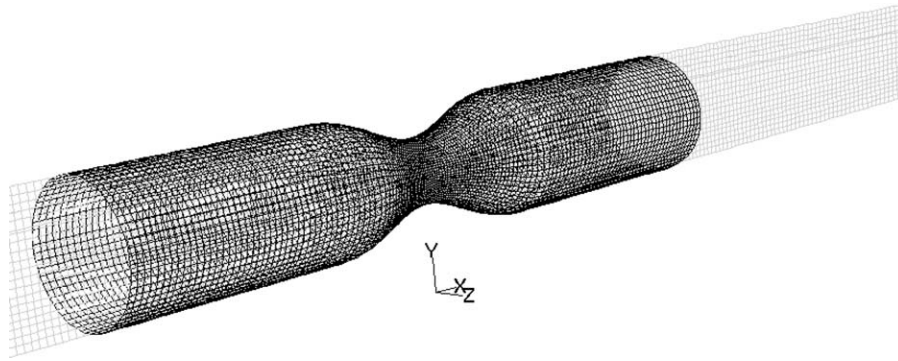


Fig. 4. Part of the 3D grid of the stenotic model, where the centre plane is also shown in lighter colour.

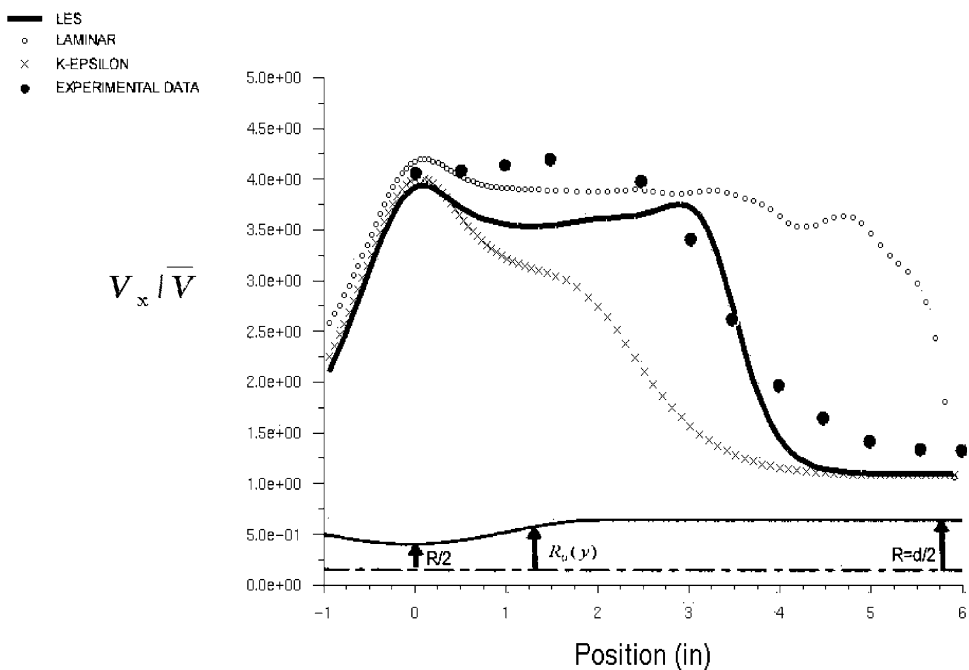


Fig. 5. Comparison of the normal centreline velocity distribution obtained using laminar, $k-\epsilon$, and LES models with the experimental data by Ahmed and Giddens [1].

experimental data), it is clear that LES indeed gives the best approximation to the experimental measurement. As particle deposition is affected mainly by large eddies, it is reasonable to assume that LES is able to provide sufficient information for calculating particle trajectories.

The particle paths of these three models are given in Fig. 6. The different degree of flow fluctuation is clearly reflected by the particle paths. The $k-\epsilon$ model has overestimated the downstream energy dissipation (not enough flow fluctuation), and laminar model underestimated it (too much flow fluctuation), because the flow is inadequately resolved.

3. Results

We now present the CFD results obtained for both the 2D and 3D simple airway models.

3.1. Two-dimensional results

Typical instantaneous velocity contours for the 2D LES model are presented in Fig. 7.

Fig. 7 shows a highly asymmetric velocity flow field in the two main bronchi. Flow stagnation occurs at the tip of the bifurcation, and extensive flow separations are seen near the outer walls of both bronchi.

The corresponding pressure contours for the LES model are shown in Fig. 8. It is noted that the pressure

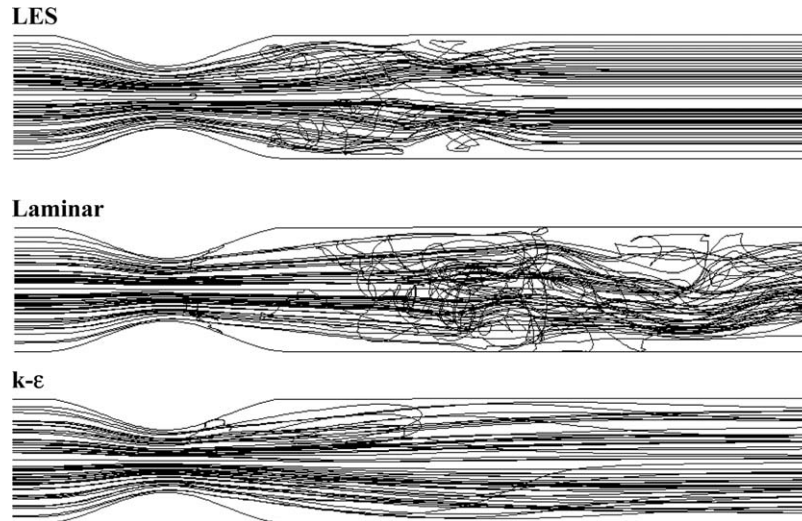


Fig. 6. The particle paths computed from LES, laminar, and $k-\epsilon$ models.

becomes negative in the both bronchi (shown by the arrow). This is obviously caused by the viscous dissipation induced by eddies.

The same results, but obtained using the laminar and $k-\epsilon$ models, are shown in Fig. 9. One very distinct difference is the lack of flow separation or eddy formation that was captured using the LES model.

3.2. Three-dimensional results

Typical instantaneous velocity contours for the 3D LES model are presented in Fig. 10. As in the 2D LES

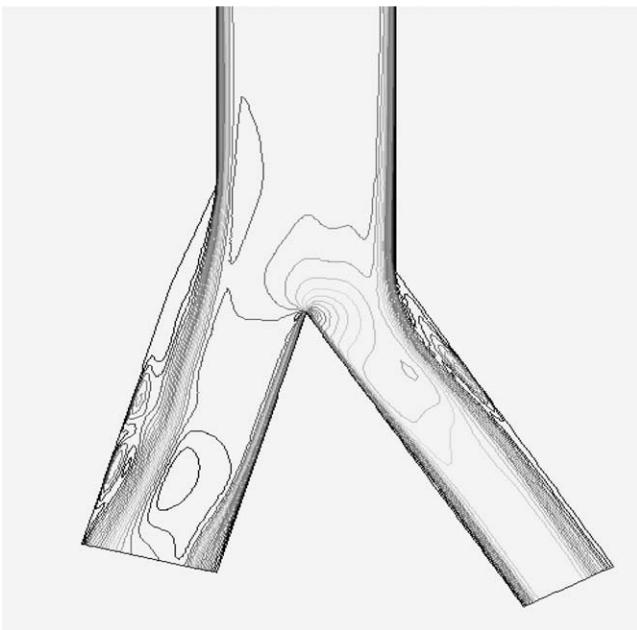


Fig. 7. 2D LES instantaneous velocity contours. The 20 of contour values are equally spaced between 0 and 2.62 m/s, the maximum velocity.

simulations, the greater flow velocities occur in the left (bigger) bronchus.

A horseshoe velocity profile develops in the right daughter bronchus, and there is little evidence of eddy formation in the left bronchus compared to the 2D simulation.

The corresponding 3D velocities are also shown for the laminar and $k-\epsilon$ models in Fig. 11. It is noted that LES is the only model that has captured the flow features such as the horseshoe pattern in the right bronchus and the skewed axial velocity distribution on left daughter branch. However, the flow patterns in the 3D models seem to suggest that the 3D flow is much less turbulent than its 2D counterpart. This will be discussed later.

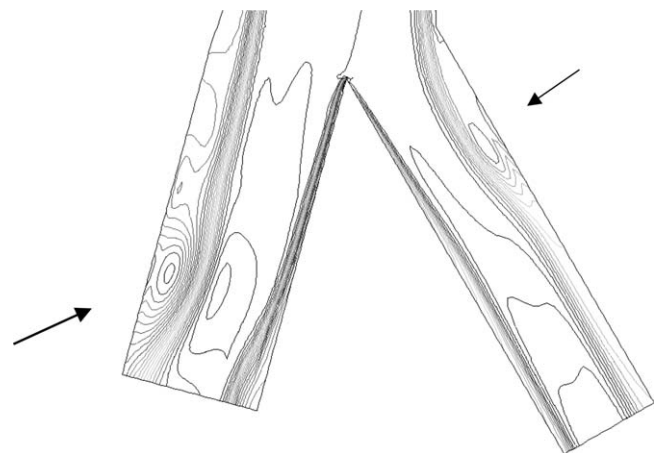


Fig. 8. Instantaneous pressure contour plots. The 20 of contour values are equally spaced between -1.5 and 4.47 Pa. Contours with negative values are located inside the recirculation area indicated by the arrow.

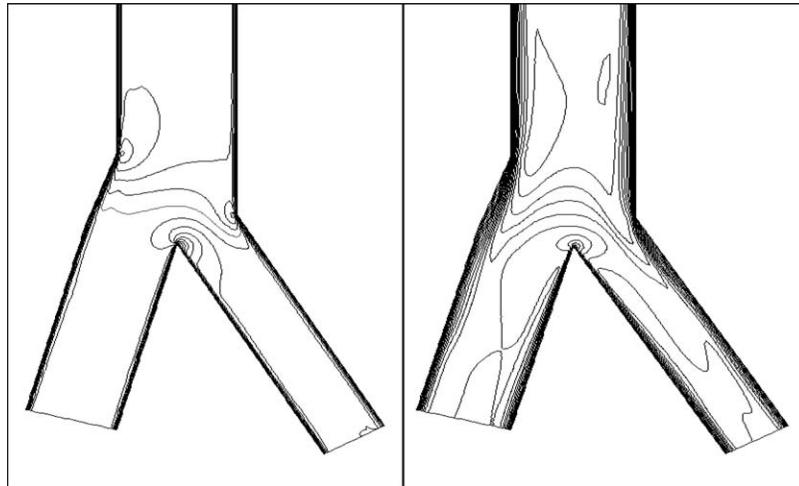


Fig. 9. The velocity contours for the (left) laminar, and (right) $k-\epsilon$ models. The 20 contour values are equally spaced between 0 and 2.62 m/s. The maximum velocities for the laminar and $k-\epsilon$ models are 2.54 and 2.38 m/s, respectively.

3.3. Particle paths

Although we are interested in the particle deposition, we cannot yet solve for the particle trajectories using the LES approach with Fluent 5, so we look at massless particle paths in the flow. These tracer particles are released from the inlet to the trachea.

3.3.1. Two-dimensional paths

The particle paths for the 2D simulations are shown in Fig. 12. It is not surprising to see that the laminar and $k-\epsilon$ models show similar trajectories. Since both the laminar and $k-\epsilon$ models cannot capture eddies in the flow, the path lines predicted by these two models

simply follow the daughter tubes. However, with the LES model, the particle paths appear to be wavering around the area of eddies.

3.3.2. Three-dimensional paths

The 3D paths are shown in Fig. 13 for the LES, laminar and $k-\epsilon$ models.

The paths from the LES show a wavering pattern in the right bronchus, whereas this is more or less smeared out in the laminar and $k-\epsilon$ models. It is clear that particles released from the entrance end up at very different places if different flow models are used. LES is likely to give a more accurate prediction of particle deposition in the upper airway.

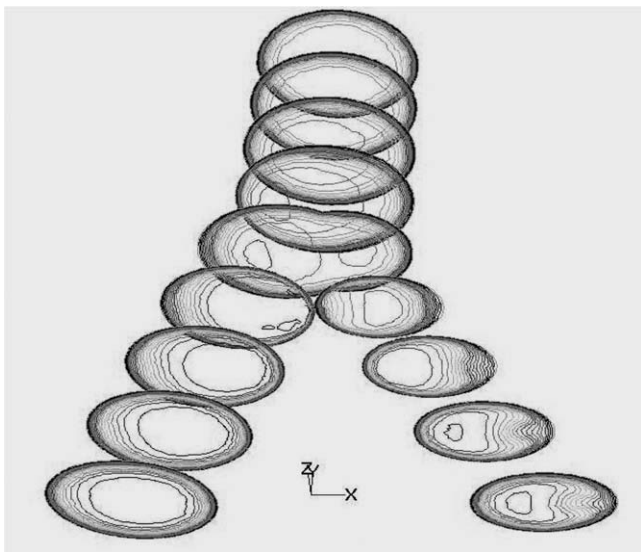


Fig. 10. The 3D LES instantaneous velocity contours at 20 equal intervals between 0 and 3.0 m/s. The maximum velocity is 2.89 m/s.

4. Discussion

In the 2D simulations, the flow pattern obtained using the LES model is much more detailed than those from the laminar and $k-\epsilon$ models. Flow separation and eddies are clearly seen in both bronchi. This is important since it is the instantaneous flow patterns, not averaged flow characteristics, that affect the particle paths and their subsequent deposition.

The 3D model seems to possess fewer significant turbulent features than the 2D model for the same entry Reynolds number. We attempt to explain this as follows. In the 2D model, $A_1 < (A_2 + A_3)$, while in the 3D case, A_1 is slightly greater than $(A_2 + A_3)$. Thus, for the same inlet flow condition, the area of 2D model expands, while the area of 3D model contracts. This fundamental difference leads to two essentially different mathematical models. Thus highlights the difficulty of employing a 2D approach to a 3D flow problem.

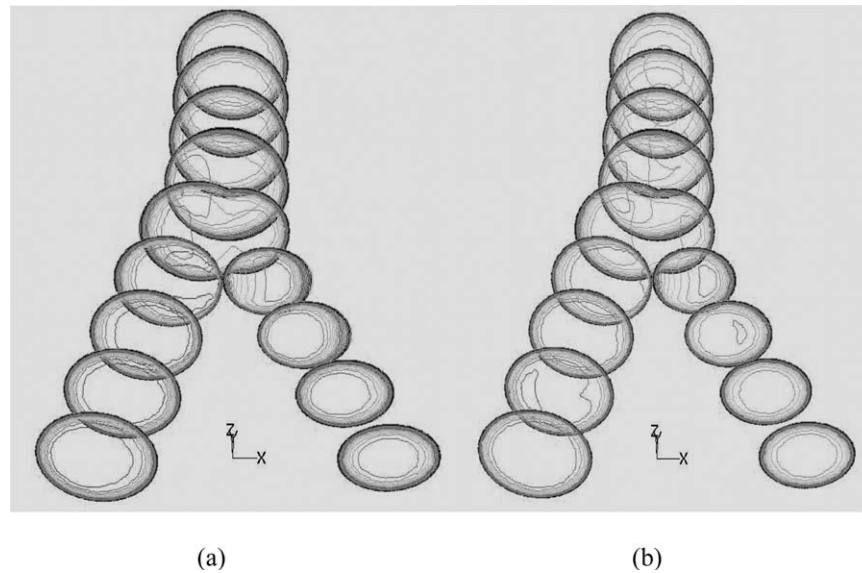


Fig. 11. The 20 velocity contours with their values equally spaced between 0 and 3.0 m/s for (a) the laminar model, where the maximum velocity is 2.75 m/s, and (b) the $k-\epsilon$ model, where the maximum velocity is 2.6 m/s.

In this study, the steady plots are only an approximation of what may happen to an inhaled particle under these flow conditions. In the LES model, the particle paths are uniform within the trachea. However, crossing of path lines is clearly visible as soon as the flow enters the bifurcation region. The most pronounced feature occurs as the flow enters the daughter bronchi in the 2D model, where the paths become more disturbed and a particle-void region is created at the flow separation zone. At this particle-void region, no particles are deposited because the particle paths are

displaced and diverted into the core flow, which prevents the particles impacting on the wall due to inertia.

Although most particles tend to be deposited in the lower order daughter branches, the fluid disturbances initiated at the entrance of the right bronchi will propagate downstream. According to Olsen et al. [30], the flow disturbances may persist for several generations of bronchial airways before becoming attenuated. Thus to assess the downstream particle deposition pattern, it is important to simulate upstream disturbances properly.

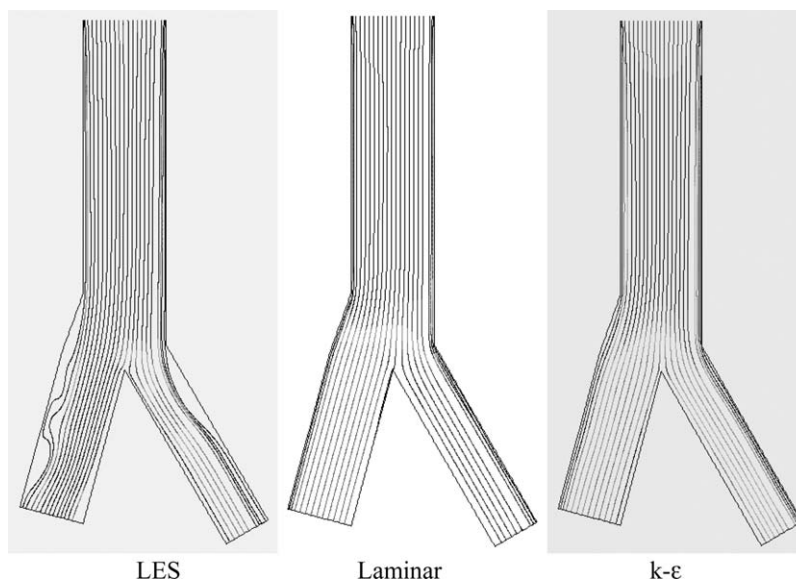


Fig. 12. 2D particle path lines predicted by the three models.

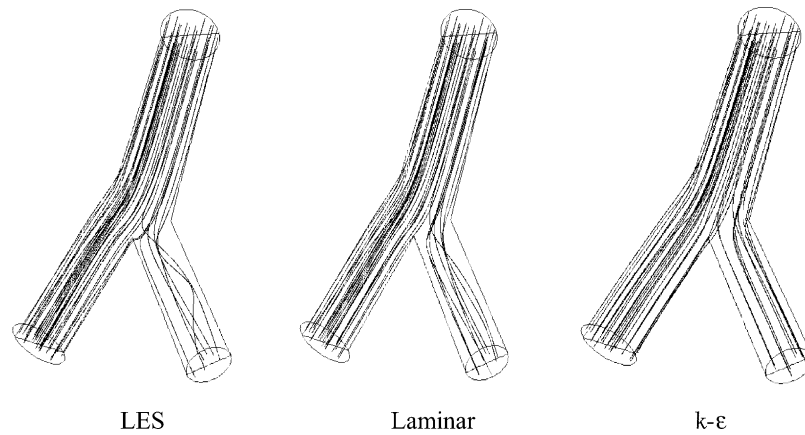


Fig. 13. 3D particle path lines from the three models.

4.1. Comparison with previous investigations

Despite the asymmetry in this model, the 2D laminar results obtained here appear to be in agreement with the 2D numerical simulations of laminar and turbulent flows in a single symmetrical bifurcation by Grotberg [9]. The turbulent results are less consistent as the separation and recirculation found in the asymmetric model are not present in the symmetrical model to the same degree.

For the 3D models, we can only compare the results qualitatively with the flow visualisation of a symmetrical bifurcation tube flow by Pedley [31]. Our results are found to be consistent with his results. The flow into each daughter tube induces secondary motion and separation depending on the corner sharpness, while boundary layer growth occurs downstream of the carina ridge. Both these features can be viewed in Fig. 10. The asymmetric nature of this model may account for the lack of separation in the left bronchus.

The results are also found to agree qualitatively with the studies by Martonen et al. [25–27], although their 3D bifurcation model is again symmetrical and their Reynolds number is lower ($=1250$). There is a good agreement in the velocity contour maps. Both studies indicate a horseshoe flow pattern in the daughter tubes with a central area of slow moving fluid.

4.2. Limitations and context

As the LES simulations are extremely time consuming, a simplified geometry is used for the airway model in this paper. Therefore, important effects, such as the laryngeal constriction and successive downstream bifurcations, on the turbulent flow are not considered. These should be accounted for in future work. Also, in the present study, our concerns are primarily focused on modelling the transitional or turbulent flows;

detailed dispersion and deposition patterns of inhaled particles are not studied. The particle paths simulated here can only be used as a crude prediction of the dispersion of particles under turbulence. Although the flow pattern is very important in determining the dispersion and deposition of particles, the particle motion would naturally depend on physical characteristics of the inhaled aerosols, such as their physical dimensions, electric and hygroscopic properties. Once these are all considered, then a more realistic deposition pattern can be simulated, and applied to the delivery of airborne drugs.

5. Conclusions

In this study, the capability of LES in modelling the transitional/turbulent flow in a simple airway model is investigated, and results are compared with the conventional $k-\epsilon$ and laminar approaches. The results indicate that LES is capable of modelling the physics of transitional/turbulent flow in the upper airway. LES allows the capture of instantaneous variable values, and can produce detailed flow patterns.

The flow in the 3D bifurcation geometry is less turbulent than its 2D counterpart for the same Reynolds number, indicating that the differences in geometry can heavily influence the nature of the flow.

It is noted that simulating the tracer particle paths can only crudely assess particle deposition. Our ultimate goal is to combine the LES turbulence model with a particle trajectory simulation, such as kinematic simulation, as a subgrid for the LES [29]. This, when applied with a more realistic model geometry, can serve as a useful tool in determining the particle deposition pattern in the upper respiratory tract of the human airways.

Appendix A. Details of LES modelling

In the LES modelling, the filtering operation for a variable $\phi(x)$, is provided by:

$$\bar{\phi}(x) = \frac{1}{V} \int_V \phi(x') G(x, x') dx' \quad (\text{A.1})$$

where V is the volume of a computational cell, and the filter function $G(x, x')$ is defined as:

$$G(x, x') = \begin{cases} 1 & \text{for } x' \in V \\ 0 & \text{otherwise} \end{cases} \quad (\text{A.2})$$

Hence the filtered Navier–Stokes equations are:

$$\frac{\partial \bar{u}_i}{\partial x_i} = 0 \quad (\text{A.3})$$

and

$$\frac{\partial}{\partial t} (\rho \bar{u}_i) + \frac{\partial}{\partial x_j} (\rho \bar{u}_i \bar{u}_j) = \frac{\partial}{\partial x_j} \left(\mu_{\text{eff}} \frac{\partial \bar{u}_i}{\partial x_j} \right) - \frac{\partial \bar{P}}{\partial x_i} \quad (\text{A.4})$$

where \bar{u}_i ($i = 1, 3$) is the filtered velocity component, x_i ($i = 1, 3$) is the coordinate, \bar{P} is the filtered pressure, t is time, ρ is the fluid density, and μ_{eff} is the effective viscosity, which is unknown, and requires modelling. In this paper, a RNG-based subgrid-scale model is used to determine μ_{eff}

$$\mu_{\text{eff}} = \mu \left[1 + H \left(\frac{\mu_s^2 \mu_{\text{eff}}}{\mu^3} - C \right) \right]^{1/3} \quad (\text{A.6})$$

where

$$\mu_s = \left(C_{\text{rng}} V^{1/3} \right)^2 \sqrt{2 \bar{S}_{ij} \bar{S}_{ij}},$$

$$\bar{S}_{ij} = \frac{1}{2} \left(\frac{\partial \bar{u}_i}{\partial x_j} + \frac{\partial \bar{u}_j}{\partial x_i} \right)$$

and H is the Heaviside function

$$H(x) = \begin{cases} x, & x > 0 \\ 0, & x \leq 0. \end{cases} \quad (\text{A.7})$$

The parameters in the model are determined to be $C_{\text{rng}} = 0.157$, $C = 100$ from the RNG theory [36].

In the high turbulent regions of flow, the RNG-based subgrid reduces to the more basic Smagorinsky–Lily model [22,32], which is suitable for a homogenous isotropic turbulence. In the low Reynolds number regions, the Heaviside function in (A.7) enables the RNG model to recover molecular viscosity, so that $\mu_{\text{eff}} = \mu$, therefore is better for modelling the low Reynolds effects encountered in transitional flows and near-wall regions.

References

- [1] Ahmed SA, Giddens DP. Velocity measurement in steady flow through axisymmetric stenoses at moderate Reynolds number. *J Biomech* 1983;16:505–16.
- [2] Balashazy I, Hofmann W, Martonen TB. Inspiratory particle deposition in airway bifurcation models. *J Aerosol Sci* 1991;22:15–30.
- [3] Balashazy I, Hofmann W. Particle deposition in airway bifurcations. 1. Inspiratory flow. *J Aerosol Sci* 1993;24:722–45.
- [4] Balashazy I, Hofmann W, Heistracher T. Computation of local enhancement factors for the quantification of particle deposition patterns in airway bifurcations. *J Aerosol Sci* 1999;30:185–203.
- [6] Darquenne C, Paiva M. One-dimensional simulation of aerosol transport and deposition in the human lung. *J Appl Physiol* 1994;77(6):2889–98.
- [7] Deshpande MD, Giddens DP, Mabon RF. Steady laminar flow through modelled vascular stenoses. *J Biomech* 1976;9:165–74.
- [8] Dekker E. Transition between laminar and turbulent flow in the human trachea. *J Appl Physiol* 1961;16:1060.
- [9] Grotberg JB. Respiratory fluid mechanics and transport processes. *Annu Rev Biomed Eng* 2001;3:421–57.
- [10] Finlay WH, Stapleton KW, Yokota J. On the use of computational fluid dynamics for simulating flow and particle deposition in the human respiratory tract. *J Aerosol Med* 1996;9:329–41.
- [11] Fluent 5.3 users' guide. Fluent Inc.; 1998.
- [12] Hofmann W, Balashazy I. Particle deposition within airway bifurcation. *Staub-Reinhalt Luft* 1991;33:178–82.
- [13] Hu ZW, Luo XY, Luo KH. Numerical Simulation of Particle Dispersion in a Spatially-Developing Mixing Layer. *J Theor Comput Fluid Dyn* 2002;15:403–20.
- [14] Kim SC, Iglesias JA. Deposition of inhaled particles in bifurcating airway models: 1. Inspiratory deposition. *J Aerosol Med* 1989;2:1–14.
- [15] Kim SC, Fisher DM, Lutz DJ, Gerrity TR. Particle deposition in bifurcating airway models with varying airway geometry. *J Aerosol Sci* 1993;25:567–81.
- [16] Koblinger L, Hofmann W. Analysis of human lung morphometric data for stochastic aerosol deposition calculations. *Phys Med Biol* 1985;30:541–56.
- [17] Koblinger L, Hofmann W. Monte Carlo modelling of aerosol deposition in human lungs. Part 1: simulation of particle transport in a stochastic lung structure. *J Aerosol Sci* 1990;21:661–74.
- [18] Lee JW, Goo JH. Numerical simulation of airflow and inertial deposition of particles in a bifurcating channel of square cross-section. *J Aerosol Med* 1992;5:131–54.
- [19] Lee JW, Goo JH, Chung MK. Characteristics of inertial deposition in a double bifurcation. *J Aerosol Sci* 1996;27:119–38.
- [20] Lighthill MJ. *Mathematical biofluidynamics*, CBMS-NSF. J.W. Arrowsmith Ltd; 1989.
- [21] Ling W, Chung JN, Troutt TR, Crowe CT. Direct numerical simulation of a three-dimensional temporal mixing layer with particle dispersion. *J Fluid Mech* 1998;358:61–85.
- [22] Lily DK. On the application of the eddy viscosity concept in the inertial subrange of turbulence. NCAR Manuscript 123, 1966.
- [24] Marcu B, Meiburg E. The effect of streamwise braid vortices on the particle dispersion in a plane mixing layer. I. Equilibrium points and their stability. *Phys Fluids* 1996;8:715–33.
- [25] Martonen TB, Yang Y. Simulation of aerosol deposition in extrathoracic and laryngeal passages of the laboratory rat. *J Aerosol Sci* 1993;24:103–13.
- [26] Martonen TB, Guan X, Shreck RM. Fluid dynamics in airway bifurcations: 1. Primary flows. *Inhalation Toxicol* 2001;13:261–79.

- [27] Martonen TB, Guan X, Shreck RM. Fluid dynamics in airway bifurcations: 2. Secondary currents. *Inhalation Toxicol* 2001; 13:281–9.
- [28] Martonen TB, Guan X, Shreck RM. Fluid dynamics in airway bifurcations: 3. Localised flow conditions. *Inhalation Toxicol* 2001;13:291–305.
- [29] Nicolleau F, Vassilicos JC. Turbulent diffusion in stably stratified non-decaying turbulence. *J Fluid Mech* 2000;410:123–46.
- [30] Olsen DE, Sudlow MF, Horsfield K, Filey GP. Convective patterns of flow during inspiration. *Arch Int Med* 1973;131:51–7.
- [31] Pedley TJ. Pulmonary fluid dynamics. *Ann Rev Fluid Mech* 1977;9:229–74.
- [32] Smagorinsky J. General circulation experiments with the primitive equations. I. The basic experiments. *Mon Wea Rev* 1963; 91:99–164.
- [33] Schlesinger RB, Lippmann M. Particle deposition in casts of the human upper tracheobronchial tree. *Am Ind Hyg Assoc J* 1972;33:237–51.
- [34] Schreck RM. Laminar flow through bifurcations with applications to the human lung. Thesis. Northwestern University, Evanston (IL), 1972.
- [35] Smith FT. On entry-flow effects in bifurcating blocked or constricted tubes. *J Fluid Mech* 1976;78:709–36.
- [36] Yokhot A, Orszag SA, Yakhot V, Israeli M. Renormalization group formulation of large-eddy simulation. *J Sci Comp* 1989;4:139–58.
- [37] Zhang Z, Kleinstreuer C, Kim CS. Micro-particle transport and deposition in a human oral airway model. *Aerosol Sci* 2002;33:1635–52.